This is a preprint, the final version is subject to change, of the American Mineralogist (MSA)
Cite as Authors (Year) Title. American Mineralogist, in press.
(DOI will not work until issue is live.) DOI: http://dx.doi.org/10.2138/am-2017-5735

Formation of the ferruginous smectite SWa-1 by alteration of soil clays

Leslie L. Baker

Department of Geological Sciences

and Department of Plant, Soil, and Entomological Sciences

University of Idaho

Moscow, ID 83844-3022

lbaker@uidaho.edu

Revision 2

This is a preprint, the final version is subject to change, of the American Mineralogist (MSA)
Cite as Authors (Year) Title. American Mineralogist, in press.
(DOI will not work until issue is live.) DOI: http://dx.doi.org/10.2138/am-2017-5735

Abstract

Clay minerals found in and near the surface of Mars contain unique information about the geochemical environment in the martian near-surface in the ancient past. In order to interpret this information, it is necessary to fully understand the environments in which different clay minerals form. Studies of terrestrial analog materials and environments are a useful way to address such questions, and some terrestrial materials are also important standards for remote sensing and in situ chemical and mineralogical analyses. This study presents new information on the formation environment of an unusual standard clay, the Clay Minerals Society source clay SWa-1 ferruginous smectite of Grant County. The SWa-1 collection locality is in the Columbia River Basalts (CRB), at the contact between a paleosol and a capping basalt flow. Features at the contact indicate the paleosol soil was wet when the capping flow was emplaced, that lava-sediment mixing occurred, and that both the soil and the capping lava were hydrothermally altered. The soil was hydrothermally enriched in Fe, Mn, and Si. The SWa-1 sample was collected from within the altered zone, suggesting it formed through alteration of paleosol clays by addition of Fe. Similar environments are widespread in the CRB, particularly at the plateau margins, suggesting that altered clays may occur frequently at lava-sediment contacts. Such environments are likely to occur wherever basalt flows are emplaced under warm, wet conditions promoting weathering – such as Mars >3.5 Ga before the present, when clay minerals were forming at its surface. This information has important implications for the use of clay compositions to inform clay formation environments on Mars.

Keywords: nontronite, Mars, clay minerals, Columbia River Basalts, SWa-1

41 ## Introduction

42 Studies of martian meteorites first demonstrated the presence of clay minerals – likely of
43 martian origin – in these samples beginning in the 1980's (Gooding et al. 1991; Bridges and
44 Grady 2000; Bridges et al. 2001). However, major occurrences of clays on Mars were not
45 confirmed until their detection by remote sensing (Poulet et al. 2005). Further studies showed
46 that clay minerals are widespread in ancient martian rocks (Bibring et al. 2005; Bibring et al.
47 2006; Mustard et al. 2008). These observations had dramatic implications for the climatic history
48 on Mars, for they showed that ancient (>3.5 Ga) Mars must almost certainly have experienced
49 periods of the warm, wet climatic conditions that promote rock weathering to clays. Some of the
50 observed clays, particularly Fe-Mg smectites, may have formed by fluid alteration in the
51 subsurface rather than at the surface, so the observed clay mineralogy may have implications for
52 martian hydrologic cycling as well (Ehlmann et al. 2011a).

53 The types and compositions of clay minerals observed in ancient martian deposits vary,
54 as do their potential environments of formation (Bishop et al. 2008; Ehlmann et al. 2008; Wray
55 et al. 2008; McKeown et al. 2009; Murchie et al. 2009; Noe Dobrea et al. 2010; Bristow and
56 Milliken 2011; Ehlmann et al. 2011a; Ehlmann et al. 2011b; Ehlmann et al. 2013). Outcroppings
57 of Fe-Mg smectites are widespread across the planet. More aluminuous smectites also occur, as
58 does kaolinite. At some localities, stratigraphic relationships are observed between clays of
59 different compositions, suggesting the strata formed in specific types of environments. For
60 example, layering of kaolinite or Al-smectites above Fe-Mg smectites could potentially indicate
61 in-situ clay development by basalt alteration in a pedogenic environment (Loizeau et al. 2007;
62 Bishop et al. 2008; Mustard et al. 2008; Wray et al. 2008; McKeown et al. 2009; Murchie et al.
63 2009; Ehlmann et al. 2011b; Carter et al. 2015), whereas clays in obviously sedimentary deposits

such as deltas suggest possible sedimentary transport and redeposition (Loizeau et al. 2007; Michalski and Noe Dobrea 2007; Ehlmann et al. 2008; Mustard et al. 2008; McKeown et al. 2009; Milliken and Bish 2010).

The crystal chemistry of martian clays is critical to these interpretations. For example, where weathering in pedogenic environments is proposed, this is based upon a model of progressive alteration of a mafic parent rock in which early weathering produces ferromagnesian smectites, and progressive leaching at the surface removes soluble components until only relatively aluminous phases remain. Application of this to a martian context requires a full understanding of terrestrial weathering and clay formation. As the surface of Mars is largely basaltic in composition, basalt weathering systems on Earth have been targeted as potential Mars analogs (Michalski et al. 2006; Ehlmann et al. 2012; Greenberger et al. 2012; Thomson et al. 2014; Greenberger et al. 2015; Yesavage et al. 2015).

Ground-truthing of remote sensing instruments with appropriate terrestrial mineral standards is also critical to proper interpretation of remotely sensed data from Mars. Several widely used nontronite mineral standards -- including the nontronites of Garfield, Manito, and Cheney, as well as the SWa-1 ferruginous smectite – were collected from, and presumed to have been formed by, weathering of Columbia River Basalts (CRB). However, the environments in which these clays were produced are surprisingly poorly understood, having been the subject of little investigation since their original identification in the mid-20th century (Allen and Scheid 1946; Kerr and Kulp 1949; Hosterman 1960). The collection locations of standard nontronites from Cheney and Spokane (at least two independent samples from "Spokane" – possibly those of Ross and Hendricks (1945) but this is not clear) have never been described in print, and that of the SWa-1 smectite was only recently identified (Baker and Strawn 2014). The Garfield and

Manito nontronites are well located (Kerr and Kulp 1949), but their formation environments have never been closely investigated.

The SWa-1 source clay has been widely used as a nontronite standard, but its unusually aluminous composition sets it apart from most other CRB-derived nontronites (Gates et al. 2002). This study presents evidence that the unusual composition of SWa-1 is a result of its formation by alteration of a preexisting soil clay rather than directly by alteration of a basaltic parent. This type of clay alteration is likely to be widespread not only in the CRB, but in any surface environment where basaltic volcanism and wet sediments coexist. Thus, it must be considered as a potential clay-forming environment on Mars.

Methods

Field site description

The CRB are continental flood basalt lavas located in the interior northwestern United States including portions of eastern Washington, eastern Oregon, and northern Idaho (Hooper 1982). The majority of these lavas were erupted during the mid-Miocene Climatic Optimum, when the climate of the northwestern United States was considerably warmer and wetter than in the present day. Lava flows exposed at the surface weathered rapidly under these conditions to form soils. Those soils were later covered by younger lava flows, preserving them as buried paleosols that act as records of past climatic conditions (Sheldon 2003; Sheldon 2006; Takeuchi et al. 2007; Hobbs and Parrish 2016). Interbedded sediments of non-pedogenic origin, such as fluvio-lacustrine or volcanic material, are also present between flows at many localities (Smith et al. 1989; Ebinghaus et al. 2014). The degree to which the capped soil or sediment and the

capping flow appear to have interacted varies widely between localities, from no observable alteration whatsoever, to interactions ranging from discoloration of sediments and/or capping basalt through explosive mixing of basalt and sediments. This variation must have depended strongly on the amount of water in the sediments and possibly the emplacement rate of the capping basalt, but was also likely affected by other environmental factors such as soil or sediment texture.

The SWa-1 sample was originally collected in 1970 from a basalt-capped paleosol near Trinidad, WA (47°16'45" N, -119°58'59" W), as recorded in unpublished field notes by J. A Kittrick (Baker and Strawn 2014). That site was revisited for the present study. Samples were collected from an outcrop in a roadcut along Washington State Highway 28 at the Trinidad Grade. At the site, a paleosol 30-40 cm thick overlies a saprolite developed upon a flow of the Basalt of Gingko, and capped by a flow of the Basalt of Sand Hollow (both units of the Frenchman Springs Member of the Wanapum Basalts of the Columbia River Basalts) (Tolan et al. 2009). The elapsed time between emplacement of the Gingko and Sand Hollow flows is not well constrained due to the difficulty of precisely dating the basalts, but is likely to be considerably less than 1 Ma (Barry et al. 2013).

At the field site, the highway grade cuts progressively downward from the capping basalt flow into the paleosol, the saprolite, and the saprolite parent flow, so that older rocks are exposed downgrade. The capping flow exhibits features of lava-wet sediment interaction (Figure 1) including hyaloclastites, peperites, sediment-filled spiracle or pipe vesicle-like structures, and pillow-like structures. Along much of the outcrop, a discontinuous 10-50 cm thick layer of silica sinter-like material lies between the paleosol surface and the capping flow. Occasional petrified

wood is present weathering from the paleosol, and tree branch molds were observed in the capping flow.

The exposed paleosol exhibits mottling and color banding, with distinct brown, green, and white layers appearing in some locations. These layers are not continuous along the outcrop.

Sample collection

Samples were collected from several localities along the basalt-paleosol contact. At Site 1, the paleosol and overriding basalt were separated by a thick layer of green-colored silica, and the paleosol and basalt exhibited streaky brown, green, and white mottling (Figure 1e). The silica and subsamples of the brown and green clays were collected. At Site 2, the silica layer was not present, and the contact between the paleosol (35 cm thick at the sampling site) and overriding basalt was exposed (Figure 1f). Samples were collected from the paleosol immediately below the contact with the overriding basalt. Individual white, green, and brown color bands were physically separated and subsampled. A bulk sample of mottled paleosol containing all three colors was also collected. The paleosol and underlying saprolite were sampled at 10, 15, 20, 30, 60, and 80 cm below the basalt-paleosol contact.

Samples were collected using a trowel to excavate intact hand samples. The paleosol soil (0-10 cm) was coherent and was also collected in pebble-sized pieces. The coherence of the paleosol soil bore no apparent relationship to the color banding. Saprolite hand samples were coherent, and were collected with a trowel or pried loose with a rock pick depending on their hardness.

The lowermost parent basalt exposed at the transect site appeared to be lightly altered and fresh, unaltered parent basalt was not accessible from directly beneath the sampled transect.

Therefore an unweathered-appearing sample of parent basalt was collected from the same flow at a site ~30 m down-grade, from the base of an outcrop of columnar basalt.

Analytical methods

Bulk samples of all saprolite and paleosol samples, and of the parent basalt, were submitted to Bureau Veritas (Vancouver, Canada) for lithium metaborate fusion and ICP-AES analysis. Bulk paleosol, saprolite, and basalt samples and the differently colored paleosol subsamples were crushed by hand for mineralogical analysis by Fourier transform infrared spectrosopy (FTIR) and powder X-ray diffractometry (XRD). Samples of the silica layer were crushed by hand using a mortar and pestle and prepared as grain mounts for optical analysis, FTIR, and XRD. Clay fractions were separated by centrifugation from the green clay subsample from Site 1. Oriented mounts of clay separates were prepared using the method of Drever (1973). XRD scans were run on a Siemens D5000 diffractometer using a Cu Kα source, and data were analyzed using the Bruker Diffracplus Eva evaluation program. Samples for FTIR analysis were mixed with optical-grade KBr at a clay:KBr ratio of 3:100 and analyzed on a Perkin-Elmer System 2000 spectrometer with diffuse reflectance accessory. IR spectra were processed using the Kubelka-Munk algorithm provided in Perkin Elmer Spectrum 2.0 software.

Results

Bulk chemical analyses

Bulk chemical analyses of the parent basalt and saprolite samples collected from Site 2 are shown in Table 1. These data show the progressive leaching of mobile elements from the saprolite samples. At 80 cm depth, compared to the parent basalt, the majority of Mg and K had

already been leached from the rock along with some Ca, Si, and Fe. This leaching trend progressed with decreasing depth up to 20 cm. At 10-15 cm depth, Na, K, and Ca were almost entirely depleted. Calculated values for the Chemical Index of Alteration (Nesbitt and Young 1982), also shown in Table 1, reflected these element losses and were typical of progressive element losses during chemical weathering of mafic rocks. Depletion of P and Ti in the 10-15 cm samples suggested the onset of dissolution of apatite and Fe-Ti oxides at these depths. This result is somewhat unusual since Ti is frequently considered to be a conservative element during weathering (Hill et al. 2000); however, Ti mobility in individual profiles is affected by the resistance to weathering of the individual mineral phase in which it resides (Maynard 1992).

In opposition to typical chemical weathering trends of upward depletion of most elements, several elements were significantly enriched in the upper saprolite and/or the paleosol. This enrichment is more noticeable when sample compositions are considered on a volatile-free basis (Table 1). Concentrations of Fe in the paleosol and 10 and 15 cm saprolite samples exceeded Fe concentration in the lower saprolite and the parent basalt. Similarly, Si concentrations in the paleosol and the saprolite samples down to 20 cm exceeded Si concentration in the parent basalt. The Mn concentration in the saprolite was enriched to several times its value in the parent basalt. The Mg concentration in the 10 and 15 cm saprolite samples was over twice its concentration in the samples from 30-80 cm.

These enrichments are not typical of weathering trends created by progressive leaching of minerals. Such atypical surface enrichments strongly suggest that Fe, Mn, and Si were added to the paleosol and/or uppermost saprolite from an external source, superimposing a later enrichment trend on the earlier chemical patterns created by pedogenic weathering.

XRD

198 Bulk XRD of the parent basalt (Figure 2a) showed that plagioclase feldspar was the
199 major crystalline phase, consistent with published descriptions of the Gingko flow (Martin et al.
200 2013). Minor titanomagnetite was also detected. The broad peak centered near 12° 2θ arises from
201 minor interstitial glass.

202 Bulk XRD of the lower saprolite samples indicated that feldspar persisted up to 20 cm
203 below the contact before mostly disappearing, although a small relict feldspar peak was apparent
204 in the 10 cm sample. A small smectite peak at 14.3 Å appeared in the deeper saprolite samples
205 and became dominant in the 10 cm saprolite sample. A broad 7.2 Å peak, suggestive of kaolinite,
206 was present in the 20 cm saprolite sample but was very weak in the 10 cm sample. The 10 cm
207 sample also displayed broadening of the small, sharp magnetite peak evident in the lower
208 samples, probably due to dissolution of primary titanomagnetite (Table 1, Ti loss above 20 cm)
209 and precipitation of Fe (oxyhydr)oxides such as goethite.

210 Bulk analysis of a crushed sample of the paleosol indicated smectites, goethite, and minor
211 quartz. Analyses of hand-separated samples of color bands within a portion of the paleosol
212 indicated varying proportions of smectites, kaolinite, goethite, and quartz. The green-tinted silica
213 layer contained quartz with minor smectites and goethite.

214 XRD clay mineral analysis was carried out on the clay-size fraction separated from a
215 green clay subsample collected from the basalt-paleosol contact at the approximate locality of
216 the original collection of the SWa-1 sample (Figure 1e). This analysis showed the green clay was
217 a smectite (Figure 2b) with a d-spacing of 14.5 Å for the Mg-saturated clay, collapsing to 12 Å
218 upon K-saturation and to 10.3 Å upon heating of the K-saturated slide to 300°C. Expansion of
219 the clay upon glycerol solvation was minimal (to 15 Å); nontronites are typically less expansive
220 than montmorillonites (Harris and White 2008).

221 **FTIR**

222 The IR spectra of the bulk paleosol, colored paleosol layers, brown lens, green silica, and
223 10 cm saprolite samples (Figure 3) generally agreed with the major mineralogy determined by
224 XRD. FTIR peak locations and assignments are given in Table 2. The locations of stretching and
225 bending peaks are useful for distinguishing clay compositions, particularly in mixed Fe-Al
226 smectites (Gates 2005; Neumann et al. 2011). Kaolinite is also distinctive in IR spectra, with its
227 pair of OH-stretching bands at 3620 and 3700 cm^{-1}, and goethite may be distinguished by the
228 hydroxyl stretch near 3160 cm^{-1} and the bending vibrations near 895 and 795 cm^{-1} (Russell and
229 Fraser 1994).

230 The sample of green-tinted silica that was identified by XRD as containing quartz did not
231 display the characteristic sharp IR doublet at 800 and 780 cm^{-1} that is observed for crystalline
232 quartz; rather, it displayed a single, somewhat broad peak centered near 795 cm^{-1}. Such a peak is
233 more characteristic of cristobalite, tridymite, or opaline silica than of quartz (Madsen et al. 1995)
234 or moganite (Zhang and Moxon 2014). Cristobalite is ruled out by the XRD peak at 3.34 rather
235 than 4 Å. This material may be comparable to the silica sinters found in hydrothermal areas,
236 which recrystallize over time from less ordered opal phases to quartz (Herdianita et al. 2000).

237 **Optical analysis of grain mounts**

238 The green-tinted silica sample examined in grain mount had a very fine sugary texture
239 with grain sizes on the order of 100 μm. Some of these grains were rod-shaped with double
240 terminations. Similar quartz grains have been experimentally shown to form at temperatures of
241 350-550 °C from modern sediments containing silica (Wüst et al. 2008). As discussed above,

242 XRD analysis of this sample indicated that it contained quartz (Figure 2), while FTIR analysis
243 suggested a less ordered silica phase (Figure 3).

244

245 ## Discussion

246 ### Paleosol alteration model for formation of SWa-1 ferruginous smectite

247 This trend of upward depletion followed by re-enrichment is apparent on the triangle
248 diagram in Figure 4, which shows the compositions of parent basalt, saprolite and paleosol
249 samples, and a nontronite clay separate. For purposes of comparison, a published analysis of
250 SWa-1 source clay is also shown (Gates et al. 2002). The arrows labelled "1" and "2" on the
251 diagram show typical trends that would be expected from early leaching of ferromagnesian
252 minerals followed by later dissolution of feldspar. These two processes have been shown to be
253 typical for weathering and soil formation on some CRB (Thomson et al. 2014).

254 Normal soil-forming processes on a basaltic parent rock would be expected to follow the
255 chemical leaching trends labeled 1 and 2 on Figure 4. These trends describe, first the leaching of
256 Fe and Mg by dissolution of olivine and/or pyroxenes, followed by later leaching of K, Na, and
257 Ca and formation of aluminous clay minerals as a result of incongruent dissolution of feldspars.
258 The end result of these processes is a residual soil enriched in Al and depleted in more mobile
259 components. Residual Fe in the soil is typically present in the form of (oxyhydr)oxides rather
260 than as Fe silicates. Nontronite clay, while typically found in the deep saprolite, would not be
261 expected in the paleosol.

262 On Figure 4, the Trinidad saprolite samples from 20 cm and below follow trend 1. No
263 saprolite or paleosol samples analyzed define trend 2; however, the identification of

montmorillonite and kaolinite in the upper saprolite and paleosol, as well as textural evidence of feldspar dissolution at depths <20 cm, strongly suggests that the original soil formation processes followed that trend. This is in agreement with the data presented by Thomson et al. (2014) for a CRB paleosol near Craigmont, ID, where saprolite samples following trend 1 (ferromagnesian depletion) were capped by a kaolinitic paleosol that plotted at a composition close to the tip of the trend 2 arrow in Figure 4.

The Trinidad 10 and 15 cm saprolite samples, and all the paleosol samples, would therefore be expected to plot near the tip of the trend 2 arrow. The actual bulk compositions of these samples are much more aluminous than the deeper and less weathered saprolite samples, but they are also strikingly enriched in Fe and Mn with respect to those samples. This re-enrichment is most pronounced in the paleosol sample, the bulk composition of which plots very close to that of the high-iron nontronite clay separate collected from this site. The SWa-1 composition falls along a mixing line between the 10-15 cm saprolite samples and the paleosol and high-Fe nontronite sample.

This enrichment in Fe, Mn, and Si of the paleosol and uppermost saprolite samples would not be expected to arise through normal pedogenic processes. Given the obvious signs of lava-soil-water interaction at this site, it appears that this enrichment arose by leaching of Fe, Mn, and Si from the capping basalt and redeposition of these elements in the paleosol and upper saprolite. The enrichment of Fe and Si in samples 10-15 cm deep in the saprolite showed that this process did not occur directly at the contact between basalt and sediment, and therefore that transport by water was required. The mottling and banding observed in the altered sediments near the basalt-soil contact was likely controlled by variations in local porosity and permeability, or by variations in solution chemistry affecting mineral stability.

As shown on Figure 4, the bulk paleosol composition is close to that of a high-iron nontronite sample. However, XRD and FTIR results show that the paleosol contains a mixture of clays and oxides including kaolinite, montmorillonite, pyrolusite, and goethite as well as nontronite. The mottling and variations in mineralogy observed in the paleosol indicate that, even where bulk composition is similar, the mineralogy may be dominated by nontronite or it may consist of Al-clays plus goethite.

No nontronite was observed in the upper saprolite samples (Figures 2 and 3), and nontronite would not be expected in the pre-alteration paleosol. However, the SWa-1 nontronite was collected from immediately below the basalt-paleosol contact, indicating that it came from the altered paleosol. This strongly suggests that SWa-1 formed via hydrothermal alteration of aluminous paleosol clays by hot fluids charged with dissolved Fe, Mn, and Si. This origin for the SWa-1 clay provides reasonable explanations for its unusually aluminous and magnesian composition.

Conditions and timescale of alteration

Some previous studies have examined the proposed type of clay alteration. It has been proposed that the Al-rich composition of the Uley nontronite NAu-1 could result from nontronite recrystallization during kaolinitization (Keeling et al. 2000). Alteration of aluminous smectites has also been investigated in the context of nuclear waste storage and of oolitic iron ores. Aluminous clays may react with dissolved Fe(II) or with metallic Fe to form a variety of phases including ferrous saponite, berthierine, odinite, cronstedtite, and greenalite (Bhattacharyya 1983; Wilson et al. 2006b; Wilson et al. 2006a; Lanson et al. 2012).

Relatively little information exists regarding the modification of clay bulk composition by volcanism in pedogenic environments; however, it has been proposed in continental (April 1980) and seafloor (Inoue and Utada 1991; Vitali et al. 1999; Lackschewitz et al. 2000; Abad et al. 2003) sediments intruded by basaltic dikes, and in volcaniclastic sediments intruded by diorites (Inoue and Utada 1991). Experimental studies have shown that Fe exchange between nontronite clays and aqueous Fe(II) occurs within hours at room temperature (Neumann et al. 2013), suggesting that the minimum time required for significant hydrothermal alteration of clay chemistry may be very short.

Hydrothermal clay alteration at high temperature (>200 °C) has been observed to result in illitization or chloritization of smectites, and in production of other higher-temperature phases, often with an observable zonation away from the igneous contact (Inoue and Utada 1991; Lackschewitz et al. 2000) although this pattern is sometimes overprinted by cooling over time (Abad et al. 2003). The absence of higher-temperature phases or of chloritized smectites from the Trinidad paleosol suggests that alteration of the clays in this system was confined to temperatures well below 200 °C.

Emplacement of a lava flow over wet sediments would result in immediate boiling of water and quenching of lava at the contact. The presence of the heat source vertically above the water would prevent convective transport of heat from the contact into the sediments below, although lateral convection would be possible beneath non-flat portions of the contact (Nield and Bejan 2006). All soil water heated to above the boiling point would therefore migrate upwards to the paleosol-lava contact but would be unable to move further upwards, unless it was able to percolate into the overlying hot basalt flow through fractures in the chilled margin. Deeper soil water would likely be wicked upward into the dried near-contact sediments and, where

temperatures were high enough, would boil. Expansion of steam and re-condensation in cooler sediments would drive some non-convective water transport away from the lava contact. Even after temperatures dropped below the boiling point, hydrothermal circulation would be suppressed by the position of the heat source above the sediments, although fluid may have moved laterally along the paleosol-lava contact. The hot fluids would alter the capping basalt and extract soluble components from it, but transport of those components downwards into the underlying soil would be limited. This is consistent with the observation that alteration of the paleosol and saprolite is largely confined to within 15 cm of the contact, and with the absence of higher-temperature alteration.

The solubilities of both Fe and Mn are strongly controlled by oxidation state. In the reaction zone at Trinidad, a fresh basalt flow containing reduced Fe was emplaced over an oxidized soil formed under pedogenic conditions. Fluids reacting with the glassy basalt at the flow base would be buffered to reducing conditions by the basalt, increasing solubility of Fe and Mn. The initially oxidizing conditions in the paleosol and uppermost saprolite would promote oxidation and precipitation of those elements.

Origin of the silica layer

The sinter-like silica material is only found along the contact between the paleosol and the overlying flow. It forms a discontinuous layer that in places appears to finger upwards into the base of the overriding lava flow (Figure 1d). This physically distinct layer bears no apparent direct relationship to the underlying paleosol. Its presence may account for the previous identification of quartz in the unprocessed SWa-1 ferruginous smectite sample (Chipera and Bish 2001). This identification is otherwise difficult to explain because the source region is basaltic, with no other apparent source of quartz.

As discussed above, the paleosol and uppermost saprolite are enriched in Si with respect to the immediately underlying layers, and the paleosol contains more Si than the parent basalt (Table 1). This suggests the excess Si was hydrothermally deposited in the soil and upper saprolite. One possible source for this excess Si is hydrothermal leaching from the glassy base of the overriding lava flow. However, this source presents a mass balance problem. Deposition of a given volume of pure silica requires leaching of 100% of the Si from approximately twice that volume of basaltic lava, or less efficient leaching of a greater volume. Although the capping basalt at this site is clearly altered, such extensive leaching would leave a residuum enriched in elements such as Al, which is not observed.

During Wanapum time, tectonic activity in this region and the interaction of Frenchman Springs flows with the Columbia River drainage caused that river, in this region of Washington State, to form a series of interconnected lakes (Reidel and Tolan 2013; Ebinghaus et al. 2014). These lakes served as habitat for abundant diatoms; diatomites are well documented in Wanapum-aged sedimentary beds, and are economically exploited near the field site. Although the Trinidad site was wet at the time of emplacement of the capping Sand Hollow basalt, no specific evidence exists for long-term flooding of the Trinidad paleo-soil surface; however, this site may have been flooded at some point between the time of soil formation and the time of the capping flow emplacement, and the silica layer may have originally been diatomaceous in origin. If so, as no evidence for diatom structures was observed in grain mount.

As noted above, rod-shaped, doubly-terminated silica grains similar to those observed in the silica layer have been experimentally shown to form by recrystallization of biogenic silica at temperatures of 350-550°C (Wüst et al. 2008). The co-occurrence of nontronite in the green silica layer indicates that it likely did not achieve this temperature range because nontronite is

377 not stable at T > 200°C. Wüst et al. (2008) did not carry out experiments at temperatures below
378 350°C, but they suggest recrystallization of biogenic silica is likely to occur even at ambient
379 conditions, with elevated temperatures facilitating nucleation and growth of quartz crystals.

380 **Likely importance at other CRB sites**

381 Zones of lava-sediment interaction are widespread in the CRB. They are particularly
382 abundant near the distal edges of the plateau, where lava flows embaying higher topography
383 repeatedly dammed drainages, resulting in formation of short-lived lakes or wetlands and in
384 deposition of locally thick sediments between flows (Hosterman 1960; Smiley and Rember
385 1985). Towards the western edge of the plateau, thick sequences of volcaniclastic sediments
386 derived from eruptions of the Cascades volcanoes are present between flows (Smith 1988a;
387 Smith 1988b; Smith et al. 1989). Hydrothermal alteration of interbedded sediments and their
388 capping lava flows is therefore likely to be very common in CRB. The resulting mineral
389 assemblages will be a product of both the conditions of alteration and the original primary
390 mineralogy of the sediments (soil, fluviolacustrine, volcaniclastic). Further analysis of sediments
391 collected from a variety of sites will explore the possible range of final clay compositions and the
392 thickness of alteration zones, to assess the likely volumetric importance of clay minerals altered
393 by hydrothermal activity at lava flow margins.

394 A "nontronite-beidellite" clay that is unusually (for a CRB clay) rich in both Al and Fe
395 was described by Ross and Hendricks (1945) as having been found "lying between basalt flows"
396 of the CRB. This sample was collected from the area southeast of Spokane, WA, but not enough
397 location information exists to pinpoint its source. Both paleosols and sedimentary clay interbeds
398 commonly occur between basalt flows near the eastern margins of the CRB where this sample
399 was collected (Hosterman 1960). This sample therefore potentially represents an example of a

pedogenic or sedimentary clay that was later altered by hydrothermal interaction with a capping basalt flow.

Likely significance to Mars

At the time of clay formation (<3.5Ga), Mars was a volcanically active planet with an environment that may have been relatively warm and wet. In this environment, lava flow emplacement would be coeval with aqueous sediment transport and deposition, and with clay-forming surface processes such as pedogenesis. Occurrences of interbedded lava, sediment, and soil are therefore virtually certain to occur on Mars – as has been proposed for many of the observed clay outcrops. The chemistry of some of these clays could therefore have been affected by lava-sediment hydrothermal interactions as proposed here for the Trinidad paleosol. The resulting mineralogical changes could significantly change potential interpretations of clay-forming environments observed from orbit. Hydrothermal overprinting of a pedogenic sequence comparable to that observed at the Trinidad site could be marked by superposition of nontronites atop aluminous clays. In the CRB, this overprinting produces clay layering that is distinctive on a scale of centimeters to meters; such stratigraphic sequences may be difficult to distinguish from orbit, but would be easily apparent from a ground-based observing platform such as a rover.

As noted above, it is not clear whether the green silica layer at the paleosol-basalt contact is typical of this type of alteration or whether it indicates an unusually silica-rich surface sediment. Therefore, this feature is likely not a good marker to search for as an indicator of lava-sediment interaction on Mars.

It has also been proposed that early Mars was predominantly cold and icy. The CRB presents a relatively poor terrestrial analog for this type of system. However, eruption of basalt

422 onto ice-bearing sediments would be expected to provide a pulse of heat that temporarily
423 produced warm, wet conditions in the subsurface immediately underneath the lava flow and
424 around feeder dikes (Squyres et al. 1987; McKenzie and Nimmo 1999). This could lead to
425 similar patterns of alteration beneath freshly emplaced lava flows, whether the original water
426 source was liquid water or ice.

427 **Implications**

428 This study demonstrates that hydrothermal alteration of soil clays by a younger basalt
429 flow can significantly alter the original pedogenic mineralogy. The compositions of layered clays
430 on Mars likely hold important clues to the formation environments of the clay minerals. The
431 young Mars was both wet (necessary to form clays) and volcanically active (as evidenced by
432 widespread lava flows). Where lava overran wet clay sediments, these sediments could have
433 undergone local compositional modification by hydrothermal fluids. More extensive contact
434 metamorphism could have resulted in illitization or chloritization of smectites, or in production
435 of higher-temperature phases. These possibilities should be taken into account in interpretations
436 of lava-capped phyllosilicate occurrences on Mars, including higher-grade occurrences which
437 have been interpreted as products of hydrothermal alteration (Ehlmann et al. 2011a).

438 **Acknowledgements**

439 This research was funded by a seed grant from the Regents of the University of Idaho. I
440 thank Charlene Home for assistance with laboratory analyses, Ken Sprenke for assistance with
441 field sampling, and Jerry Fairley for helpful discussions regarding hydrothermal reactions below
442 a heat source. Thoughtful reviews by Liz Rampe and an anonymous reviewer significantly
443 improved the manuscript.

References cited

Abad, I., Jiménez-Millán, J., Molina, J.M., Nieto, F. and Vera, J.A. (2003) Anomalous reverse zoning of saponite and corrensite caused by contact metamorphism and hydrothermal alteration of marly rocks associated with subvolcanic bodies, Clays and Clay Minerals 51, 5, 543-554.

Allen, V.T. and Scheid, V.E. (1946) Nontronite in the Columbia River region, American Mineralogist 31, 294-312.

April, R.H. (1980) Regularly interstratified chlorite/vermiculite in contact metamorphosed red beds, Newark Group, Connecticut Valley, Clays and Clay Minerals 28, 1, 1-11.

Baker, L.L. and Strawn, D.G. (2014) Temperature effects on synthetic nontronite crystallinity and implications for nontronite formation in Columbia River Basalts, Clays and Clay Minerals 62, 2, 89-101.

Barry, T., Kelley, S., Reidel, S., Camp, V., Self, S., Jarboe, N., Duncan, R. and Renne, P. (2013) Eruption chronology of the Columbia River Basalt Group, Geological Society of America Special Papers 497, 45-66.

Bhattacharyya, D.P. (1983) Origin of berthierine in ironstones, Clays and clay minerals 31, 3, 173-182.

Bibring, J.-P., Langevin, Y., Mustard, J.F., Poulet, F., Arvidson, R., Gendrin, A., Gondet, B., Mangold, N., Pinet, P., Forget, F. and the Omega team (2006) Global Mineralogical and Aqueous Mars History Derived from OMEGA/Mars Express Data, Science 312, 5772, 400-404.

Bibring, J.-P., Langevin, Y., Gendrin, A., Gondet, B., Poulet, F., Berthé, M., Soufflot, A., Arvidson, R., Mangold, N., Mustard, J., Drossart, P. and the Omega team (2005) Mars

Surface Diversity as Revealed by the OMEGA/Mars Express Observations, Science 307, 5715, 1576-1581.

Bishop, J.L., Dobrea, E.Z.N., McKeown, N.K., Mario Parente, Ehlmann, B.L., Michalski, J.R., Milliken, R.E., Poulet, F., Swayze, G.A., Mustard, J.F., Murchie, S.L. and Bibring, J.-P. (2008) Phyllosilicate diversity and past aqueous activity revealed at Mawrth Vallis, Mars, Science 321, 830-833.

Bridges, J. and Grady, M. (2000) Evaporite mineral assemblages in the nakhlite (martian) meteorites, Earth and Planetary Science Letters 176, 3, 267-279.

Bridges, J.C., Catling, D., Saxton, J., Swindle, T., Lyon, I. and Grady, M. (2001) Alteration assemblages in martian meteorites: implications for near-surface processes, Space Science Reviews 96, 1, 365-392.

Bristow, T.F. and Milliken, R.E. (2011) Terrestrial perspective on authigenic clay mineral production in ancient martian lakes, Clays and Clay Minerals 59, 4, 339-358.

Carter, J., Loizeau, D., Mangold, N., Poulet, F. and Bibring, J.-P. (2015) Widespread surface weathering on early Mars: A case for a warmer and wetter climate, Icarus 248, 373-382.

Chipera, S.J. and Bish, D.L. (2001) Baseline studies of the Clay Minerals Society Source Clays: Powder X-ray diffraction analyses, Clays and Clay Minerals 49, 5, 398-409.

Drever, J.I. (1973) The preparation of oriented clay mineral specimens for X-ray diffraction analysis by a filter-membrane peel technique, American Mineralogist 58, 553-554.

Ebinghaus, A., Hartley, A.J., Jolley, D.W., Hole, M. and Millett, J. (2014) Lava–sediment interaction and drainage-system development in a large igneous province: Columbia River Flood Basalt Province, Washington State, USA, Journal of Sedimentary Research 84, 11, 1041-1063.

Ehlmann, B.L., Bish, D.L., Ruff, S.W. and Mustard, J.F. (2012) Mineralogy and chemistry of altered Icelandic basalts: Application to clay mineral detection and understanding aqueous environments on Mars, Journal of Geophysical Research: Planets 117, E11.

Ehlmann, B.L., Mustard, J.F., Clark, R.N., Swayze, G.A. and Murchie, S.L. (2011a) Evidence for low-grade metamorphism, hydrothermal alteration, and diagenesis on Mars from phyllosilicate mineral assemblages, Clays and Clay Minerals 59, 4, 359-377.

Ehlmann, B.L., Mustard, J.F., Murchie, S.L., Bibring, J.-P., Meunier, A., Fraeman, A.A. and Langevin, Y. (2011b) Subsurface water and clay mineral formation during the early history of Mars, Nature 479, 7371, 53-60.

Ehlmann, B.L., Mustard, J.F., Fassett, C.I., Schon, S.C., Head Iii, J.W., Des Marais, D.J., Grant, J.A. and Murchie, S.L. (2008) Clay minerals in delta deposits and organic preservation potential on Mars, Nature Geosci 1, 6, 355-358.

Ehlmann, B.L., Berger, G., Mangold, N., Michalski, J.R., Catling, D., Ruff, S.W., Chassefière, E., Niles, P.B., Chevrier, V. and Poulet, F. (2013) Geochemical Consequences of Widespread Clay Mineral Formation in Mars' Ancient Crust, Space Science Reviews 174, 1-4, 329-364.

Gates, W. (2005). Infrared spectroscopy and the chemistry of dioctahedral smectites. CMS Workshop Lectures, Clay Minerals Society.

Gates, W.P., Slade, P.G., Manceau, A. and Lanson, B. (2002) Site occupancies by iron in nontronites, Clays and Clay Minerals 50, 2, 223-239.

Gooding, J.L., Wentworth, S.J. and Zolensky, M.E. (1991) Aqueous alteration of the Nakhla meteorite, Meteoritics 26, 2, 135-143.

512 Greenberger, R.N., Mustard, J.F., Kumar, P.S., Dyar, M.D., Breves, E.A. and Sklute, E.C. (2012)
513 Low temperature aqueous alteration of basalt: Mineral assemblages of Deccan basalts
514 and implications for Mars, Journal of Geophysical Research: Planets 117, E11, n/a-n/a.
515 Greenberger, R.N., Mustard, J.F., Cloutis, E.A., Mann, P., Wilson, J.H., Flemming, R.L.,
516 Robertson, K.M., Salvatore, M.R. and Edwards, C.S. (2015) Hydrothermal alteration and
517 diagenesis of terrestrial lacustrine pillow basalts: Coordination of hyperspectral imaging
518 with laboratory measurements, Geochimica et Cosmochimica Acta 171, 174-200.
519 Harris, W. and White, G.N. (2008) X-ray diffraction techniques for soil mineral identification, In
520 Methods of Soil Analysis. Part 5. Mineralogical Methods. . Ulery, A. L. and Drees, L. R.,
521 Ed., pp. 81-115, Soil Science Society of America, Madison, WI.
522 Herdianita, N.R., Browne, P.R.L., Rodgers, K.A. and Campbell, K.A. (2000) Mineralogical and
523 textural changes accompanying ageing of silica sinter, Mineralium Deposita 35, 1, 48-62.
524 Hill, I.G., Worden, R.H. and Meighan, I.G. (2000) Yttrium: The immobility-mobility transition
525 during basaltic weathering, Geology 28, 10, 923-926.
526 Hobbs, K.M. and Parrish, J.T. (2016) Miocene global change recorded in Columbia River
527 basalt−hosted paleosols, Geological Society of America Bulletin.
528 Hooper, P.R. (1982) The Columbia River Basalts, Science 215, 4539, 1463-1468.
529 Hosterman, J.W. (1960) Geology of the clay deposits in parts of Washington and Idaho, Clays
530 and Clay Minerals 7, 285-292.
531 Inoue, A. and Utada, M. (1991) Smectite-to-chlorite transformation in thermally metamorphosed
532 volcanoclastic rocks in the Kamikita area, northern Honshu, Japan, American
533 Mineralogist 76, 3-4, 628-640.

534 Keeling, J.L., Raven, M.D. and Gates, W.P. (2000) Geology and characterization of two
535 hydrothermal nontronites from weathered metamorphic rocks at the Uley graphite mine,
536 South Australia, Clays and Clay Minerals 48, 5, 537-548.
537 Kerr, P.F. and Kulp, J.L. (1949) Reference clay localities, United States, In Reference clay
538 minerals; American Petroleum Institute research project 49. Preliminary reports no. 1-8.
539 Kerr, P. F. and Kulp, J. L., Ed., pp. 69-73, Columbia University, New York.
540 Lackschewitz, K.S., Singer, A., Botz, R., Garbe-Schönberg, D., Stoffers, P. and Horz, K. (2000)
541 Formation and Transformation of Clay Minerals in the Hydrothermal Deposits of Middle
542 Valley, Juan de Fuca Ridge, ODP Leg 169, Economic Geology 95, 2, 361-389.
543 Lanson, B., Lantenois, S., van Aken, P.A., Bauer, A. and Plançon, A. (2012) Experimental
544 investigation of smectite interaction with metal iron at 80 °C: Structural characterization
545 of newly formed Fe-rich phyllosilicates, American Mineralogist 97, 5-6, 864-871.
546 Loizeau, D., Mangold, N., Poulet, F., Bibring, J.P., Gendrin, A., Ansan, V., Gomez, C., Gondet,
547 B., Langevin, Y., Masson, P. and Neukum, G. (2007) Phyllosilicates in the Mawrth Vallis
548 region of Mars, J. Geophys. Res. 112, E8, E08S08.
549 Madsen, F.A., Rose, M.C. and Cee, R. (1995) Review of Quartz Analytical Methodologies:
550 Present and Future Needs, Applied Occupational and Environmental Hygiene 10, 12,
551 991-1002.
552 Martin, B.S., Tolan, T.L. and Reidel, S.P. (2013) Revisions to the stratigraphy and distribution of
553 the Frenchman Springs Member, Wanapum Basalt, Geological Society of America
554 Special Papers 497, 155-179.
555 Maynard, J. (1992) Chemistry of modern soils as a guide to interpreting Precambrian paleosols,
556 The Journal of Geology 279-289.

McKenzie, D. and Nimmo, F. (1999) The generation of martian floods by the melting of ground ice above dykes, Nature 397, 6716, 231-233.

McKeown, N.K., Bishop, J.L., Noe Dobrea, E.Z., Ehlmann, B.L., Parente, M., Mustard, J.F., Murchie, S.L., Swayze, G.A., Bibring, J.-P. and Silver, E.A. (2009) Characterization of phyllosilicates observed in the central Mawrth Vallis region, Mars, their potential formational processes, and implications for past climate, Journal of Geophysical Research - Planets 114, E00D10.

Michalski, J.R. and Noe Dobrea, E.Z. (2007) Evidence for a sedimentary origin of clay minerals in the Mawrth Vallis region, Mars, Geology 35, 10, 951-954.

Michalski, J.R., Kraft, M.D., Sharp, T.G. and Christensen, P.R. (2006) Effects of chemical weathering on infrared spectra of Columbia River Basalt and spectral interpretations of martian alteration, Earth and Planetary Science Letters 248, 3, 822-829.

Milliken, R.E. and Bish, D.L. (2010) Sources and sinks of clay minerals on Mars, Philosophical Magazine 90, 17-18, 2293-2308.

Murchie, S.L., Mustard, J.F., Ehlmann, B.L., Milliken, R.E., Bishop, J.L., McKeown, N.K., Noe Dobrea, E.Z., Seelos, F.P., Buczkowski, D.L., Wiseman, S.M., Arvidson, R.E., Wray, J.J., Swayze, G., Clark, R.N., Des Marais, D.J., McEwen, A.S. and Bibring, J.-P. (2009) A synthesis of Martian aqueous mineralogy after 1 Mars year of observations from the Mars Reconnaissance Orbiter, J. Geophys. Res. 114, E00D06.

Mustard, J.F., Murchie, S.L., Pelkey, S.M., Ehlmann, B.L., Milliken, R.E., Grant, J.A., Bibring, J.P., Poulet, F., Bishop, J., Dobrea, E.N., Roach, L., Seelos, F., Arvidson, R.E., Wiseman, S., Green, R., Hash, C., Humm, D., Malaret, E., McGovern, J.A., Seelos, K., Clancy, T., Clark, R., Marais, D.D., Izenberg, N., Knudson, A., Langevin, Y., Martin, T., McGuire,

P., Morris, R., Robinson, M., Roush, T., Smith, M., Swayze, G., Taylor, H., Titus, T. and Wolff, M. (2008) Hydrated silicate minerals on Mars observed by the Mars Reconnaissance Orbiter CRISM instrument, Nature 454, 7202, 305-309.

Nesbitt, H. and Young, G. (1982) Early Proterozoic climates and plate motions inferred from major element chemistry of lutites, Nature 299, 5885, 715-717.

Neumann, A., Petit, S. and Hofstetter, T.B. (2011) Evaluation of redox-active iron sites in smectites using middle and near infrared spectroscopy, Geochimica et Cosmochimica Acta 75, 9, 2336-2355.

Neumann, A., Olson, T.L. and Scherer, M.M. (2013) Spectroscopic Evidence for Fe(II)–Fe(III) Electron Transfer at Clay Mineral Edge and Basal Sites, Environmental Science & Technology 47, 13, 6969-6977.

Nield, D.A. and Bejan, A. (2006) Convection in porous media, Springer Science & Business Media.

Noe Dobrea, E.Z., Bishop, J.L., McKeown, N.K., Fu, R., Rossi, C.M., Michalski, J.R., Heinlein, C., Hanus, V., Poulet, F., Mustard, R.J.F., Murchie, S., McEwen, A.S., Swayze, G., Bibring, J.P., Malaret, E. and Hash, C. (2010) Mineralogy and stratigraphy of phyllosilicate-bearing and dark mantling units in the greater Mawrth Vallis/west Arabia Terra area: Constraints on geological origin, Journal of Geophysical Research - Planets 115, E00D19.

Poulet, F., Bibring, J.P., Mustard, J.F., Gendrin, A., Mangold, N., Langevin, Y., Arvidson, R.E., Gondet, B. and Gomez, C. (2005) Phyllosilicates on Mars and implications for early martian climate, Nature 438, 7068, 623-627.

602 Reidel, S.P. and Tolan, T.L. (2013) The late Cenozoic evolution of the Columbia River system in
603 the Columbia River flood basalt province, Geological Society of America Special Papers
604 497, 201-230.
605 Ross, C.S. and Hendricks, S.B. (1945) Minerals of the montmorillonite group, their origin and
606 relation to soils and clays. Washington, DC. US Geological Survey Professional Paper
607 205-B.
608 Russell, J.D. and Fraser, A.R. (1994) Infrared Methods, In Clay Mineralogy: Spectroscopic and
609 Chemical Determinative Methods. Wilson, M. J., Ed., pp. 11-67, Chapman & Hall,
610 London.
611 Sheldon, N.D. (2003) Pedogenesis and geochemical alteration of the Picture Gorge subgroup,
612 Columbia River basalt, Oregon, Geological Society of America Bulletin 115, 11, 1377-
613 1387.
614 Sheldon, N.D. (2006) Using paleosols of the Picture Gorge Basalt to reconstruct the middle
615 Miocene climatic optimum, PaleoBios 26, 2, 27-36.
616 Smiley, C. and Rember, W. (1985) Composition of the Miocene Clarkia flora, Late Cenozoic
617 history of the Pacific Northwest 95, 112.
618 Smith, G.A. (1988a) Sedimentology of proximal to distal volcaniclastics dispersed across an
619 active foldbelt: Ellensburg Formation (late Miocene), central Washington, Sedimentology
620 35, 6, 953-977.
621 Smith, G.A. (1988b) Neogene synvolcanic and syntectonic sedimentation in central Washington,
622 Geological Society of America Bulletin 100, 9, 1479-1492.

623 Smith, G.A., Bjornstad, B.N. and Fecht, K.R. (1989) Neogene terrestrial sedimentation on and
624 adjacent to the Columbia Plateau; Washington, Oregon, and Idaho, Geological Society of
625 America Special Papers 239, 187-198.
626 Squyres, S.W., Wilhelms, D.E. and Moosman, A.C. (1987) Large-scale volcano-ground ice
627 interactions on Mars, Icarus 70, 3, 385-408.
628 Takeuchi, A., Larson, P.B. and Suzuki, K. (2007) Influence of paleorelief on the Mid-Miocene
629 climate variation in southeastern Washington, northeastern Oregon, and western Idaho,
630 USA, Palaeogeography, Palaeoclimatology, Palaeoecology 254, 3, 462-476.
631 Thomson, B.J., Hurowitz, J.A., Baker, L.L., Bridges, N.T., Lennon, A.M., Paulsen, G. and
632 Zacny, K. (2014) The effects of weathering on the strength and chemistry of Columbia
633 River Basalts and their implications for Mars Exploration Rover Rock Abrasion Tool
634 (RAT) results, Earth and Planetary Science Letters 400, 130-144.
635 Tolan, T.L., Martin, B.S., Reidel, S.P., Kauffman, J.D., Garwood, D.L. and Anderson, J.L.
636 (2009) Stratigraphy and tectonics of the central and eastern portions of the Columbia
637 River Flood-Basalt Province: An overview of our current state of knowledge, Field
638 Guides 15, 645-672.
639 Vitali, F., Blanc, G., Larqué, P., Duplay, J. and Morvan, G. (1999) Thermal diagenesis of clay
640 minerals within volcanogenic material from the Tonga convergent margin, Marine
641 Geology 157, 1–2, 105-125.
642 Wilson, J., Savage, D., Cuadros, J., Shibata, M. and Ragnarsdottir, K.V. (2006a) The effect of
643 iron on montmorillonite stability. (I) Background and thermodynamic considerations,
644 Geochimica et Cosmochimica Acta 70, 2, 306-322.

645 Wilson, J., Cressey, G., Cressey, B., Cuadros, J., Ragnarsdottir, K.V., Savage, D. and Shibata,
646 M. (2006b) The effect of iron on montmorillonite stability. (II) Experimental
647 investigation, Geochimica et Cosmochimica Acta 70, 2, 323-336.
648 Wray, J.J., Ehlmann, B.L., Squyres, S.W., Mustard, J.F. and Kirk, R.L. (2008) Compositional
649 stratigraphy of clay-bearing layered deposits at Mawrth Vallis, Mars, Geophysical
650 Research Letters 35, 12, L12202.
651 Wüst, R., Bustin, R.M. and Ross, J. (2008) Neo-mineral formation during artificial coalification
652 of low-ash — mineral free-peat material from tropical Malaysia-potential explanation for
653 low ash coals, International Journal of Coal Geology 74, 2, 114-122.
654 Yesavage, T., Thompson, A., Hausrath, E.M. and Brantley, S.L. (2015) Basalt weathering in an
655 Arctic Mars-analog site, Icarus 254, 219-232.
656 Zhang, M. and Moxon, T. (2014) Infrared absorption spectroscopy of SiO2-moganite, American
657 Mineralogist 99, 4, 671-680.

658

659

660 **Figure captions**

661 Figure 1. Photos of field site at Trinidad, WA, USA. (a) Plumes of sediment mixed throughout
662 overlying basalt flow. (b and c) Sediment plumes containing pillow-like pods of basalt, altered to
663 goethite in photo (c). (d) Sampling site 1, showing green silica layer with discontinuous
664 thickness along contact between paleosol and overriding basalt flow.(e) Green and brown
665 mottled clays immediately below light-toned silica layer, at contact with paleosol. (f) Sampling
666 site 2 (transect), with top end of measuring tape (1 m of tape shown) marking base of lava flow
667 contact with underlying paleosol; silica layer is not present at this site.

668

669 Figure 2. Upper: Bulk powder XRD scans of saprolite and paleosol samples. Lower: Clay XRD
670 scans of green clay separate from site 1.

671

672 Figure 3. FTIR scans of saprolite and paleosol samples. Peak assignments are given in Table 2.

673

674 Figure 4. Triangle plot showing progressive changes in bulk chemistry of saprolite and paleosol
675 samples (black circles). Labels show sample depth in cm; B is parent basalt; P is paleosol. Also
676 shown are composition of a green clay separate (Trinidad) and published composition of SWa-1
677 (Gates et al. 2002).

678

Table 1. Bulk compositions in weight percent of basalt, saprolite and paleosol samples, and calculated chemical index of alteration (Nesbitt and Young, 1982).

Sample	SiO_2	Al_2O_3	Fe_2O_3	MgO	CaO	Na_2O	K_2O	TiO_2	P_2O_5	MnO	Sum	LOI	CIA
T 0 P	59.22	5.19	18.96	0.95	1.11	0.02	0.03	0.34	0.05	0.75	99.95	13.2	99
T 10 cm	46.60	13.58	15.47	1.94	2.92	0.71	0.08	0.53	0.03	0.02	99.95	18.0	79
T 15 cm	45.75	13.76	16.43	1.77	3.03	0.84	0.08	0.49	0.05	0.03	99.95	17.7	80
T 20 cm	48.13	21.67	3.33	1.46	5.70	2.62	0.31	5.02	1.15	0.06	99.82	10.2	61
T 30 cm	46.54	18.80	9.31	0.92	6.39	3.14	0.35	4.39	1.02	0.17	99.87	8.7	54
T 60 cm	46.66	19.32	8.71	0.92	6.29	3.08	0.34	4.51	1.05	0.13	99.87	8.7	54
T 80 cm	46.21	17.54	11.20	1.01	6.40	3.00	0.33	4.09	0.96	0.18	99.89	8.8	52
T Bas	50.93	13.64	12.93	3.38	8.60	2.92	1.31	3.12	0.66	0.18	99.85	2.0	38

Volatile-free basis

Sample	SiO_2	Al_2O_3	Fe_2O_3	MgO	CaO	Na_2O	K_2O	TiO_2	P_2O_5	MnO
T 0 P	68.24	5.98	21.85	1.09	1.28	0.02	0.03	0.39	0.06	0.86
T 10 cm	56.84	16.57	18.87	2.37	3.56	0.87	0.10	0.65	0.04	0.02
T 15 cm	55.60	16.72	19.97	2.15	3.68	1.02	0.10	0.60	0.06	0.04
T 20 cm	53.62	24.14	3.71	1.63	6.35	2.92	0.35	5.59	1.28	0.07
T 30 cm	50.99	20.60	10.20	1.01	7.00	3.44	0.38	4.81	1.12	0.19
T 60 cm	51.12	21.17	9.54	1.01	6.89	3.37	0.37	4.94	1.15	0.14
T 80 cm	50.68	19.24	12.28	1.11	7.02	3.29	0.36	4.49	1.05	0.20
T Bas	51.97	13.92	13.19	3.45	8.78	2.98	1.34	3.18	0.67	0.18

Table 2. FTIR band assignments for clay minerals (Neumann et al 2011; Gates 2008) and goethite (Russell and Fraser 1994). Goethite bands are indicated with the notation (G).

	OH-stretching		Si-O stretching	OH-bending			
	AlAlOH	**FeFeOH**		**AlAlOH**	**AlFeOH**	**FeFeOH**	**FeMgOH**
Brown mottle		3160 (G)	1100, 1024			895, 800 (G)	
Paleosol brown		3550 (clay), 3160 (G)	1105, 1020			885, 800 (G)	795
Paleosol green		3565	1105, 1024	915	875	815	
Paleosol white	3696, 3650, 3620		1115, 1037, 1005	915	875		795
Bulk paleosol		3565	1095, 1032		878	815	795
Green silica		3565	1225, 1095, 1032		875	823	795
Saprolite 10 cm	3624	3565	1105, 1024	915	875		780

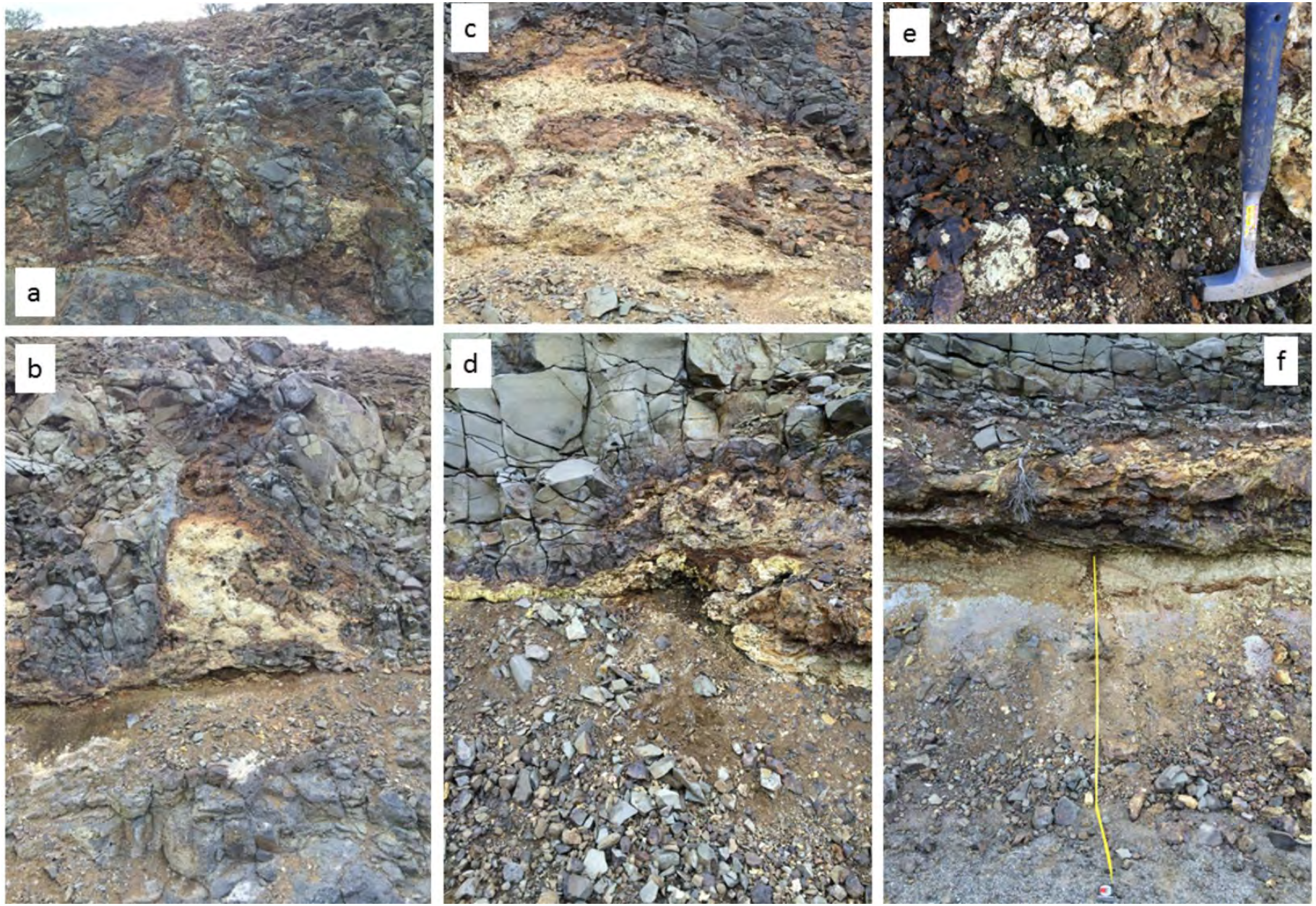

Figure 1

Figure 2a

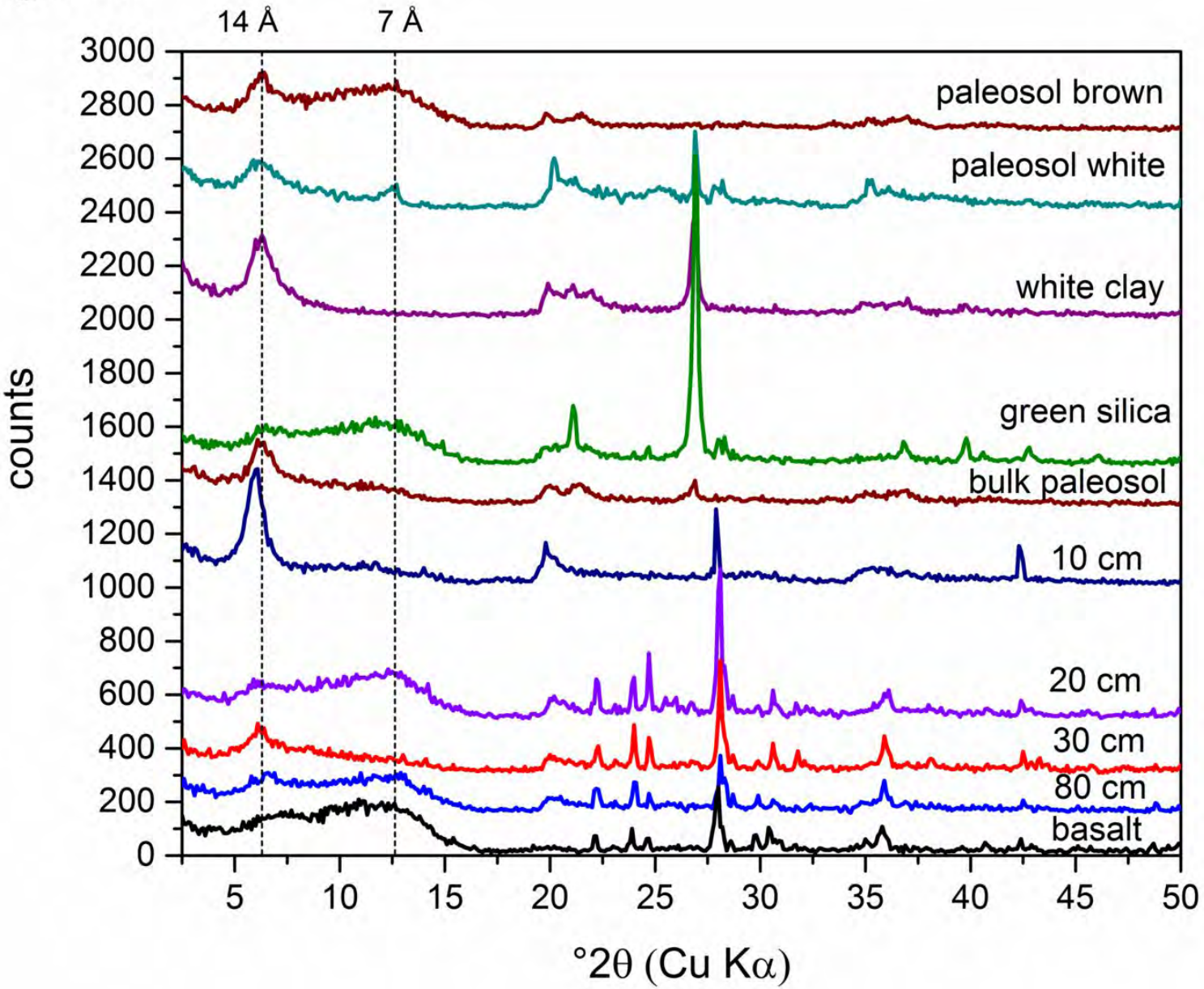
14 Å
7 Å
paleosol brown
paleosol white
white clay
green silica
bulk paleosol
10 cm
20 cm
30 cm
80 cm
basalt
counts
°2θ (Cu Kα)
0
200
400
600
800
1000
1200
1400
1600
1800
2000
2200
2400
2600
2800
3000
5
10
15
20
25
30
35
40
45
50

Figure 2b

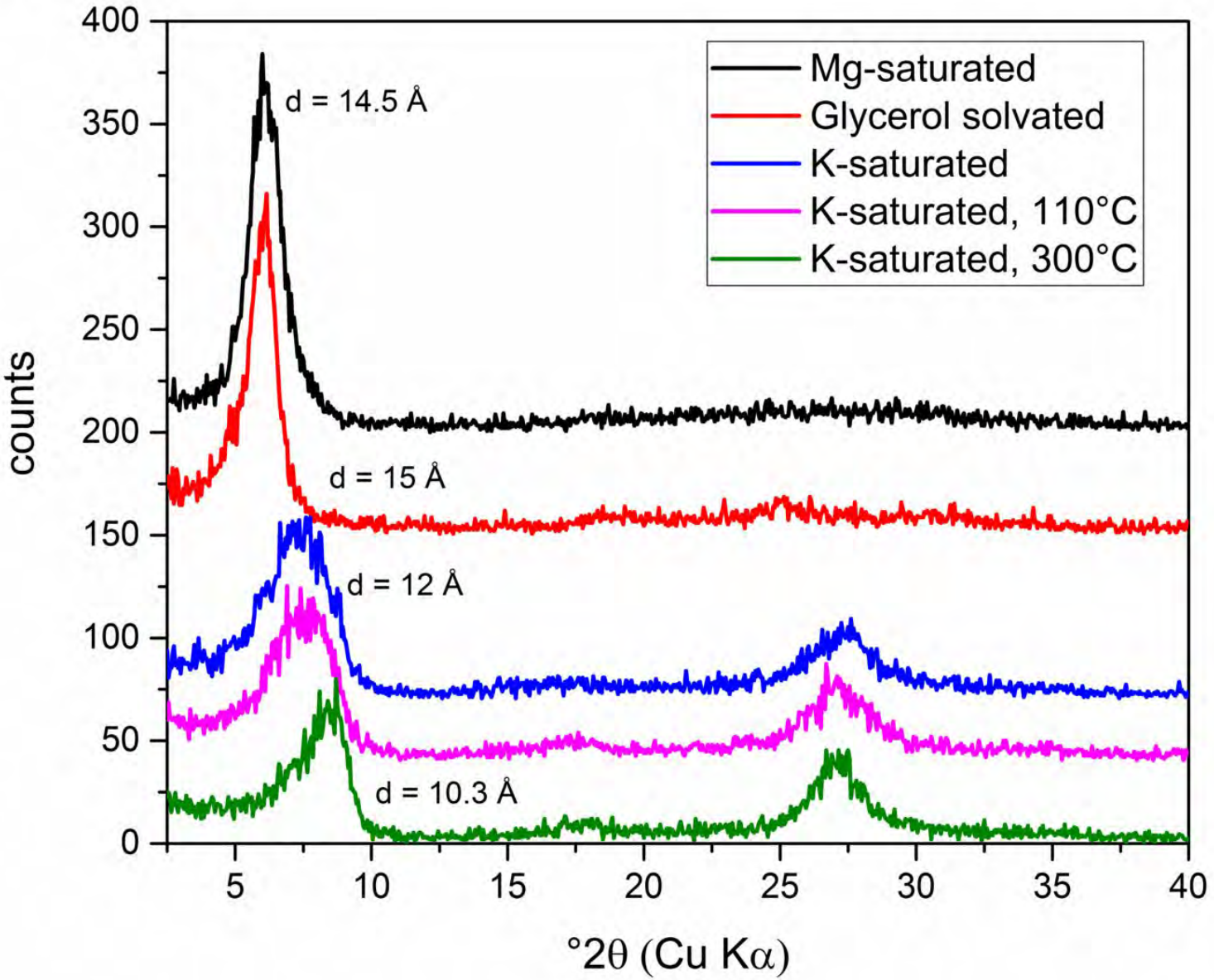
Mg-saturated
Glycerol solvated
K-saturated
K-saturated, 110°C
K-saturated, 300°C
d = 14.5 Å
d = 15 Å
d = 12 Å
d = 10.3 Å
counts
°2θ (Cu Kα)
0
50
100
150
200
250
300
350
400
5
10
15
20
25
30
35
40

Figure 3

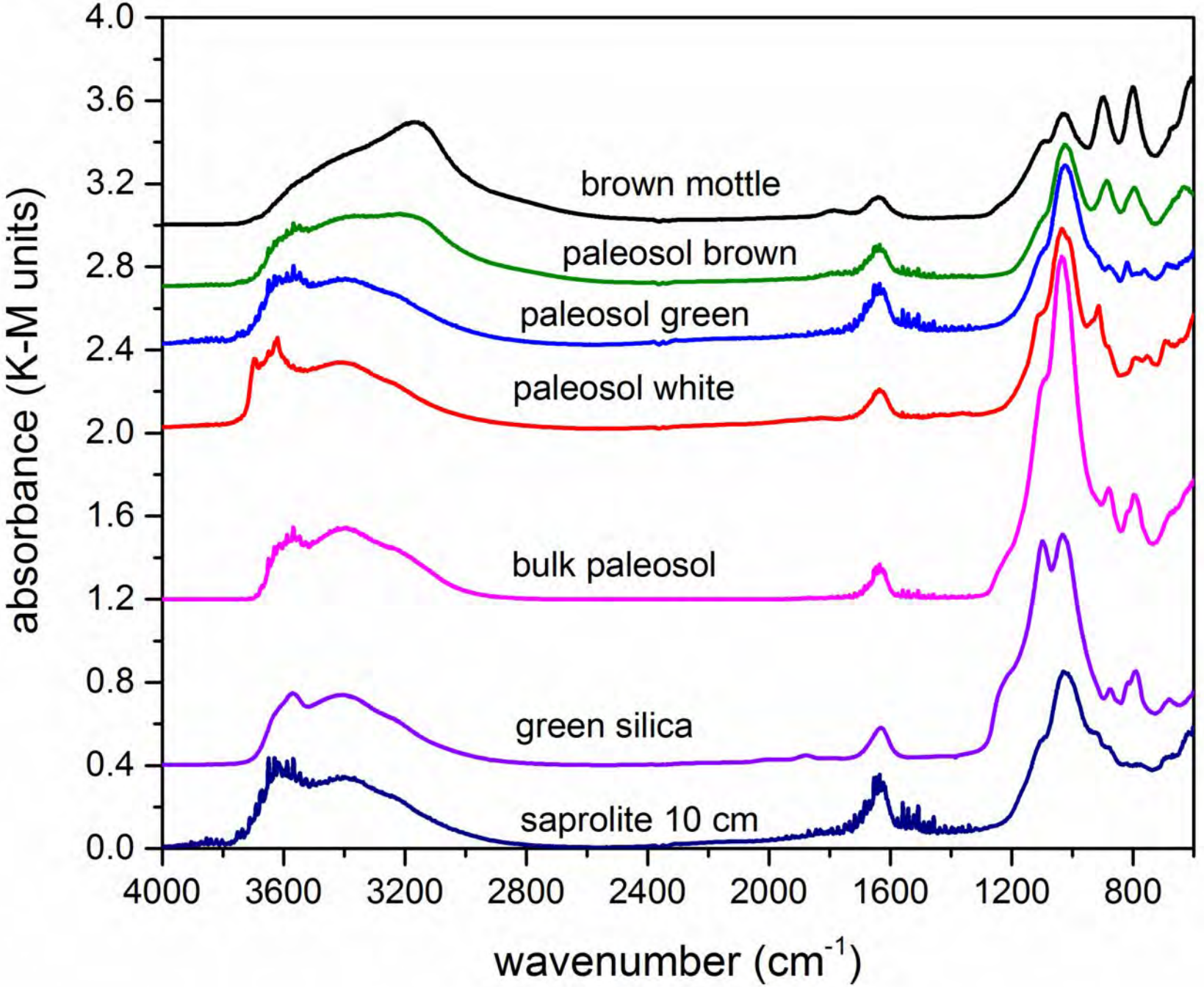
4.0
3.6
3.2
2.8
2.4
2.0
1.6
1.2
0.8
0.4
0.0
absorbance (K-M units)
brown mottle
paleosol brown
paleosol green
paleosol white
bulk paleosol
green silica
saprolite 10 cm
4000
3600
3200
2800
2400
2000
1600
1200
800
wavenumber (cm-1)

Figure 4

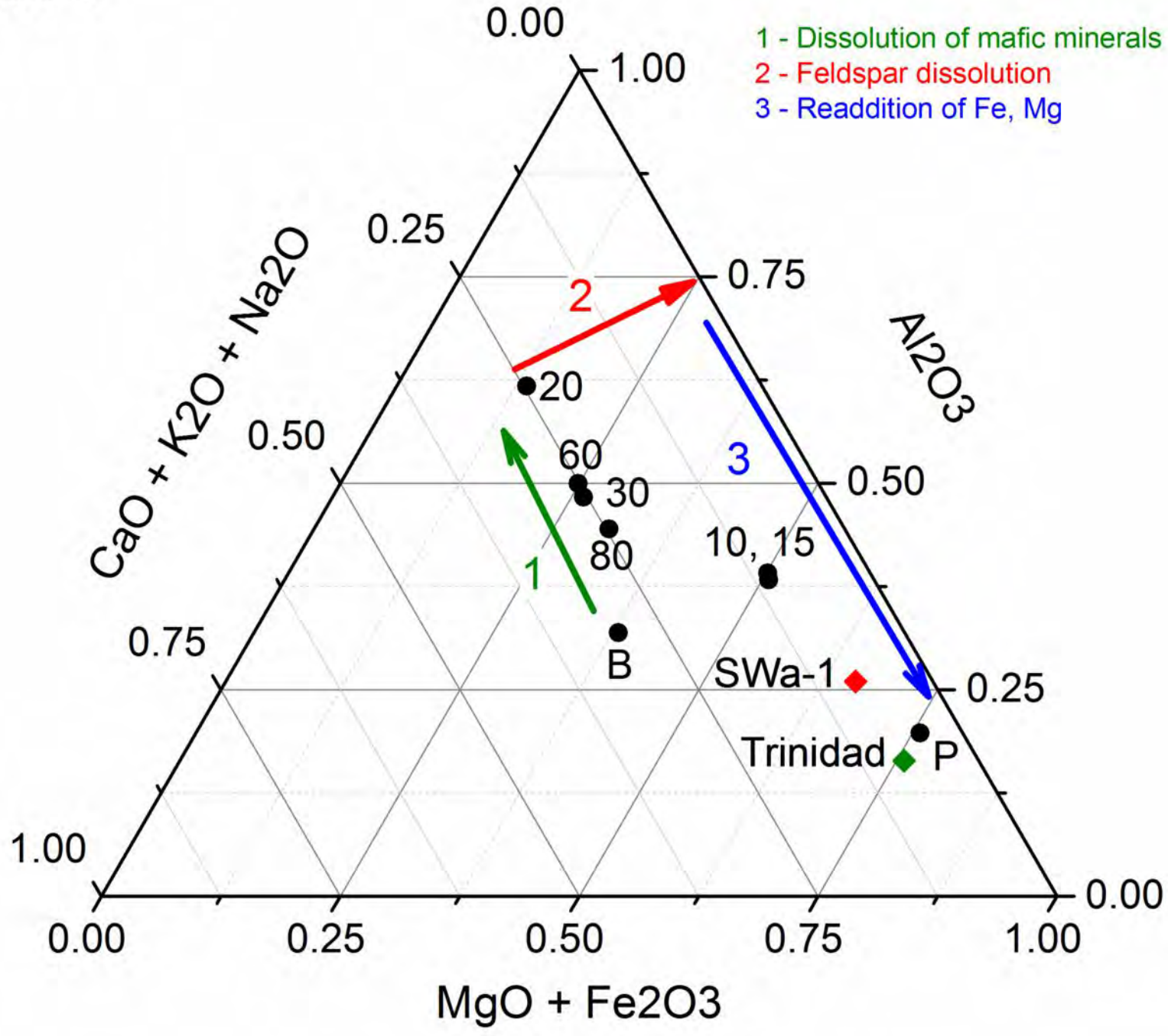
1 - Dissolution of mafic minerals
2 - Feldspar dissolution
3 - Readdition of Fe, Mg
0.00
1.00
0.25
0.75
0.50
0.50
0.75
0.25
1.00
0.00
0.00
0.25
0.50
0.75
1.00
CaO + K2O + Na2O
Al2O3
MgO + Fe2O3
2
3
1
20
60
30
80
10, 15
B
SWa-1
Trinidad
P